Electronic Supplementary Material (ESI) for Journal of Materials Chemistry A.

Predicting the Na^+ Ion Transport Properties of NaSICON Materials Using Density Functional Theory and Kinetic Monte Carlo

Judith Schuett,[a,b] Antonia S. Kuhn,[b] Steffen Neitzel-Grieshammer[b]

[a.] Helmholtz-Institut Münster (IEK-12), Forschungszentrum Jülich GmbH, Corrensstraße 46, 48149 Münster, Germany.

[b.] Institute of Physical Chemistry, RWTH Aachen University, Landoltweg 2, 52056 Aachen, Germany.

Supporting Information

1. Investigation of dependency of external electric field on conductivity

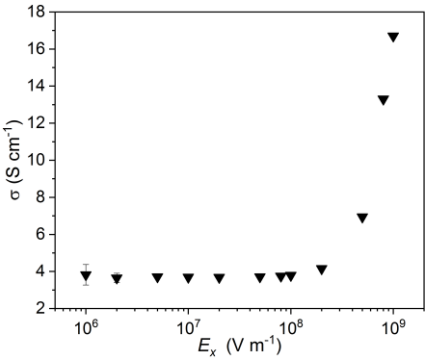

Figure S1. Sodium ion conductivity σ in dependence of electric field strength E_x in *x*-direction. In this study $E = 10^7$ Vm^{-1} was applied. Values taken from [1].

2. Volume relaxation, ionic distances, and pair interaction energies

Lattice relaxation for primitive rhombohedral cells of composition $Na_1M_2P_3O_{12}$ (M = Zr^{4+}, Hf^{4+}, Sn^{4+}) with 42 atoms was performed by DFT with an energy cut-off of 520 eV. As shown in Fig. S2, the lattice parameter *a* and volume *V* of $Na_1M_2P_3O_1$ increase with the size of the M-cation in accordance with the literature.[2–8] Here, only the lattice parameter *a* is shown, which is identical to the lattice parameters *b* and *c* in the primitive cell.

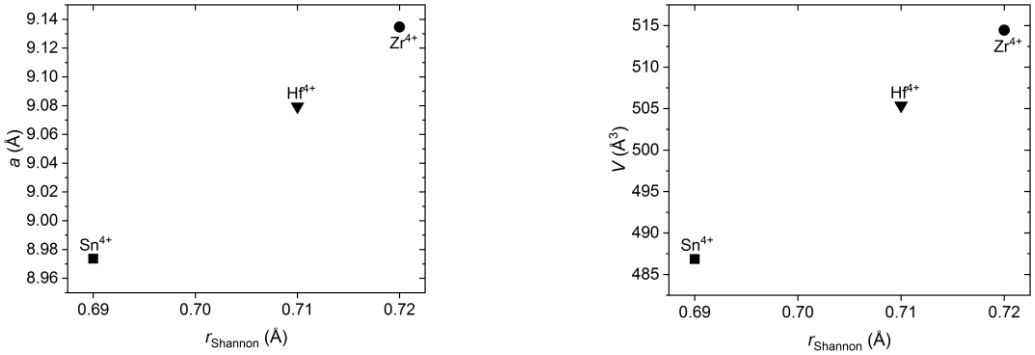

(a) Lattice parameter *a* (b) Volume *V*

Figure S2. (a) Lattice parameter *a* and (b) volume *V* of rhombohedral primitive with composition $Na_1M_2P_3O_{12}$ (M = Zr^{4+}, Hf^{4+}, Sn^{4+}) in dependence of Shannon radii $r_{Shannon}$ of *M*-cations.

3. Pair interaction energies

To determine the Na^+ site energies for any configuration of the compositions $Na_{1+x}M_2Si_xP_{3-x}O_{12}$ (M = Zr^{4+}, Hf^{4+}, Sn^{4+}), the Na2–Na2 and Na2–Si^{4+} pair interaction energies, E_{Na} and E_{Si}, were calculated depending on the Na2–cation distances. Therefore, a pair of a Na^+ ion and another cation (Na^+ or Si^{4+}) are introduced into the unsubstituted cell (x = 0) to investigate the pair interactions individually without considering addition effects. The introduction of a Si^{4+} ion on a P^{5+} site creates a -1 charged defect, while the introduction of a Na^+ ion on a vacant Na2 site corresponds to a +1 charged defect. The pair interaction between the cations is calculated relative to the cell with the furthest Na2–cation distance. Various pair interaction energies for different distances are obtained. Table S1 shows the interaction energies E_{Na} of Na2–Na2 pairs in distance $d_{Na2–Na2}$ and Table S2 shows the interaction energies E_{Si} of Na2–Si pairs in distance $d_{Na2–Si}$ for $Na_1M_2P_3O_{12}$ with M = Zr^{4+}, Hf^{4+}, Sn^{4+}. The repulsive Na2–Na2 pair interactions increase Na^+ site energies whereas the attractive Na2–Si pair interactions decrease Na^+ site energies. The pair interactions energies weaken with the distance.

Table S1. Na2–Na2 distances $d_{Na2-Na2}$ and corresponding interaction energies E_{Na} for $Na_1M_2P_3O_{12}$ with M = Zr^{4+}, Hf^{4+}, Sn^{4+}.

M = Zr^{4+}		M = Hf^{4+}		M = Sn^{4+}	
$d_{Na2–Na2}$ (Å)	E_{Na} (eV)	$d_{Na2–Na2}$ (Å)	E_{Na} (eV)	$d_{Na2–Na2}$ (Å)	E_{Na} (eV)
4.84	0.18	4.81	0.20	4.73	0.26
4.84	0.18	4.82	0.20	4.74	0.27
4.89	0.16	4.86	0.18	4.75	0.30
4.89	0.16	4.86	0.18	4.75	0.30
4.94	0.27	4.92	0.29	4.88	0.33
4.95	0.27	4.93	0.28	4.89	0.31
4.95	0.26	4.93	0.28	4.89	0.38
4.95	0.26	4.93	0.29	4.90	0.31
5.14	0.13	5.10	0.14	4.97	0.18
5.14	0.13	5.11	0.14	4.97	0.18
5.60	0.15	5.56	0.17	5.47	0.24
5.60	0.15	5.56	0.17	5.47	0.25
7.07	0.11	7.06	0.12	6.93	0.17
7.24	0.12	7.20	0.13	7.03	0.16
7.24	0.12	7.20	0.13	7.04	0.16
7.24	0.12	7.20	0.13	7.05	0.15
7.25	0.12	7.20	0.13	7.05	0.15
7.92	0.14	7.87	0.15	7.51	0.19
7.95	0.14	7.90	0.15	7.54	0.19
8.32	0.08	8.28	0.09	8.21	0.11
8.32	0.08	8.50	0.10	8.41	0.11
8.55	0.09	8.54	0.10	8.41	0.11
8.55	0.09	8.83	0.06	8.71	0.09
8.58	0.09	8.85	0.07	8.73	0.07
8.58	0.09	8.88	0.08	8.74	0.08
8.87	0.05	8.88	0.06	8.75	0.11
8.88	0.06	8.94	0.06	8.81	0.07
8.88	0.06	8.99	0.09	8.83	0.09
8.89	0.06	9.16	0.04	9.01	0.05
8.93	0.07	9.17	0.05	9.03	0.07

$M = Zr^{4+}$		$M = Hf^{4+}$		$M = Sn^{4+}$	
$d_{Na2–Na2}$ (Å)	E_{Na} (eV)	$d_{Na2–Na2}$ (Å)	E_{Na} (eV)	$d_{Na2–Na2}$ (Å)	E_{Na} (eV)
8.93	0.05	9.23	0.04	9.09	0.06
8.93	0.06	9.27	0.06	9.12	0.03
8.93	0.07	9.78	0.08	9.69	0.09
8.98	0.06	10.4	0.06	10.2	0.07
8.98	0.06	11.1	0.06	10.9	0.08
9.05	0.06	11.6	0.04	11.5	0.08
9.21	0.05	11.8	0.04	11.5	0.06
9.21	0.03	12.3	0.00	11.6	0.05
9.21	0.03	15.3	0.00	13.4	0.00
9.21	0.05	16.4	0.00	15.1	0.00
9.29	0.02			16.2	0.00
9.29	0.02				
9.33	0.06				
9.33	0.06				
9.82	0.07				
9.82	0.07				
10.5	0.05				
10.5	0.05				
11.1	0.06				
11.2	0.06				
11.4	0.04				
11.4	0.05				
11.7	0.04				
11.7	0.06				
11.8	0.04				
12.6	0.02				
13.4	0.00				
13.4	0.03				
13.9	0.01				
15.1	0.00				
16.5	0.00				
17.3	0.00				

Table S2. Si–Na2 distances $d_{Na2\text{-}Si}$ and corresponding interaction energies E_{Si} of $Na_1M_2P_3O_{12}$ with $M = Zr^{4+}$, Hf^{4+}, Sn^{4+}.

$M = Zr^{4+}$		$M = Hf^{4+}$		$M = Sn^{4+}$	
$d_{Na2–Si}$ (Å)	E_{Si} (eV)	$d_{Na2–Si}$ (Å)	E_{Si} (eV)	$d_{Na2–Si}$ (Å)	E_{Si} (eV)
2.91	-0.30	2.88	-0.36	2.83	-0.77
2.92	-0.30	2.88	-0.36	2.83	-0.78
3.04	-0.34	3.03	-0.39	3.02	-0.52
3.56	-0.26	3.54	-0.30	3.55	-0.40
3.56	-0.26	3.54	-0.30	3.56	-0.41
5.77	-0.16	5.73	-0.18	5.65	-0.19
5.94	-0.20	5.90	-0.21	5.85	-0.21

$M = Zr^{4+}$		$M = Hf^{4+}$		$M = Sn^{4+}$	
$d_{Si–Na2}$ (Å)	E_{Si} (eV)	$d_{Si–Na2}$ (Å)	E_{Si} (eV)	$d_{Si–Na2}$ (Å)	E_{Si} (eV)
5.94	-0.20	5.90	-0.21	5.85	-0.20
6.02	-0.21	5.99	-0.22	5.92	-0.27
6.02	-0.21	5.99	-0.22	5.92	-0.26
6.11	-0.18	6.07	-0.19	6.01	-0.20
6.11	-0.18	6.07	-0.19	6.01	-0.20
6.34	-0.07	6.29	-0.08	6.22	-0.14
6.43	-0.12	6.38	-0.14	6.34	-0.20
6.43	-0.12	6.39	-0.14	6.34	-0.20
6.49	-0.17	6.45	-0.18	6.38	-0.22
6.49	-0.16	6.45	-0.18	6.39	-0.22
6.75	-0.13	6.70	-0.14	6.63	-0.19
6.75	-0.13	6.71	-0.14	6.63	-0.21
7.30	-0.10	7.26	-0.11	7.18	-0.13
7.30	-0.10	7.75	-0.09	7.18	-0.14
7.79	-0.08	7.86	-0.12	7.62	-0.13
7.90	-0.12	7.97	-0.05	7.84	-0.15
7.91	-0.11	7.99	-0.08	7.92	-0.09
8.03	-0.04	8.21	-0.08	7.92	-0.09
8.06	-0.07	8.30	-0.09	8.15	-0.10
8.25	-0.07	9.55	-0.08	8.19	-0.13
8.26	-0.07	9.63	-0.04	9.42	-0.07
8.35	-0.08	9.63	-0.04	9.46	-0.07
8.35	-0.08	9.78	-0.05	9.48	-0.05
9.58	-0.05	9.79	-0.05	9.48	-0.07
9.58	-0.04	9.79	-0.06	9.67	-0.05
9.60	-0.08	9.85	-0.05	9.67	-0.06
9.60	-0.08	14.4	0.00	9.69	-0.07
9.69	-0.04	15.0	0.00	9.72	-0.06
9.69	-0.04	15.6	0.00	10.5	-0.03
9.84	-0.05			10.6	-0.05
9.85	-0.04			10.6	-0.05
9.85	-0.04			14.3	0.00
9.91	-0.04			14.8	0.00
10.7	-0.03			15.4	0.00
10.7	-0.03				
10.8	-0.07				
10.8	-0.06				
10.8	-0.04				
12.7	-0.04				
13.5	-0.05				
13.7	-0.02				
14.5	0.00				
15.1	0.00				
15.7	0.00				

Additionally, the fully substituted cells (x = 3) with composition $Na_{1+x}M_2Si_xP_{3-x}O_{12}$ in which one P^{5+} was introduced creating one vacant Na2 site (V_{Na}) were also calculated. The cells in which the P^{5+} is in nearest neighbour position to V_{Na} is energetically more favorable than the cell with large P^{5+}–V_{Na} distance. The energy of the configuration with smallest P^{5+}–V_{Na} distance was calculated relative to the energy of the configuration with largest P^{5+}–VNa distance for all compositions (M = Zr^{4+}, Hf^{4+}, Sn^{4+}) (Table S3). The results show the expected trend: The configurational energy is lowered by Si^{4+} near the Na2 positions (i.e., at large P^{5+}–VNa distance).

Table S3. Relative configurational energy of cells with smallest P^{5+}–V_{Na} distance. Cells of composition $Na_4M_2Si_3O_{12}$ (M = Zr^{4+}, Hf^{4+}, Sn^{4+}) in which one P^{5+} was introduced creating one vacancy on Na2 site (V_{Na}) were calculated.

M	E_{rel} (eV)
Zr^{4+}	-0.23
Hf^{4+}	-0.26
Sn^{4+}	-1.18

The Coulomb interactions between the two Na^+ ions as well as between Na^+ and Si^{4+} ions were calculated according to Eq. 1. Therefore, the averaged Born effective charges $\bar{q}_B$ of Na^+ ions on Na2 sites, P^{5+} and Si^{4+} on P^{5+} sites, as well as the relative permittivity ϵ_r of $Na_1M_2P_3O_{12}$ (M = Zr^{4+}, Hf^{4+}, Sn^{4+}) with two additional Na^+ ions and with one additional Na^+ and Si^{4+} ion were determined by Density Functional Perturbation Theory (DFPT). The averaged Born effective charge of the substituted P^{5+} lattice site $\bar{q}_{B,rel}$ was calculated according to Eq. 2. The Born effective charge of the Na2 site occupied by Na^+ substituent corresponds to the averaged Born effective charge of the introduced Na^+ ions $\bar{q}_{B,Na2}$ since the original Na2 site is vacant.

Table S4. Born effective charge $\bar{q}_B$ of Na2 ions and relative permittivity $\bar{\epsilon}_r$ of $Na_1M_2P_3O_{12}$ (M = Zr^{4+}, Hf^{4+}, Sn^{4+}) with two additional Na^+ ions calculated with DFPT.

M	$\bar{q}_{B,Na2(1)}/e$	$\bar{q}_{B,Na2(2)}/e$	$\bar{\epsilon}_r$ (A s V^{-1} m^{-1})
Zr^{4+}	1.02	1.06	11.12
Hf^{4+}	1.03	1.03	10.22
Sn^{4+}	1.01	1.03	10.51

Table S5. Born effective charge of Na2 ($\bar{q}_{B,Na2}$), P ($\bar{q}_{B,P}$) and Si ($\bar{q}_{B,Si}$) ions, as well as the with Si^{4+} substituted P^{5+} site ($\bar{q}_{B,rel}$), and relative permittivity $\bar{\epsilon}_r$ of $Na_1M_2P_3O_{12}$ (M = Zr^{4+}, Hf^{4+}, Sn^{4+}) with one additional Na^+ and Si^{4+} ion calculated with DFPT.

M	$\bar{q}_{B,Na2}/e$	$\bar{q}_{B,P}/e$	$\bar{q}_{B,Si}/e$	$\bar{q}_{B,rel}/e$	$\bar{\epsilon}_r$ (A s V^{-1} m^{-1})
Zr^{4+}	1.10	4.16	3.88	−0.28	9.65
Hf^{4+}	1.08	4.05	3.72	−0.33	9.36
Sn^{4+}	1.09	3.68	3.24	−0.44	7.71

4. Migration energy profiles and pathways

The correlated migration of two Na^+ ions was investigated in $Na_{1+x}M_2Si_xP_{3-x}O_{12}$ (M = Zr^{4+}, Hf^{4+}, Sn^{4+}) with x = 0 and x = 3 using Climbing Image Nudged Elastic Band (CI-NEB) method with five interpolated images. For the unsubstituted structure (x = 0), one additional Na^+ ion was introduced on the Na2 site, whereas for the fully substituted structure (x = 3), one vacancy was created by removing one Na^+ ion from the Na2 site. The resulting energy profiles of the migration paths in 80°, 90° and 180° direction are shown in Fig. S3. Our results of the 90° and 180° migration in the composition $Na_1Zr_2P_3O_{12}$ is consistent with the findings of Zou *et al*.[9] The shape of the energy profiles is similar for all compositions. However, in structures with x = 3, there is a local minimum along the migration path in the 180° direction for M = Zr^{4+} and in the 90° and 180° direction for M = Hf^{4+}. This state corresponds to the occupied mid-sodium positions located between the Na1 and Na2 site along the migration path, as observed in previous studies.[9–14] This mid-Na site only occurs at high substitution levels in structures with larger cations (M = Hf^{4+}, Zr^{4+}). In structures with smaller Sn^{4+} cations, the shorter bond distances lead to unfavorable stronger Na^+–cation repulsion and steric destabilization of the mid-Na sites. Fig. S4 shows the different coordination environments of Na^+ ions in the intermediate state (dark green) along the migration pathway (light green) defined by the adjacent O^{2-}. Therefore, in the compound with M = Sn^{4+} the intermediate state poses the transition state. But in the compounds with larger cations (M = Hf^{4+}, Zr^{4+}), the mid-Na site corresponds to a local minimum, which may further facilitate the migration of Na^+ ions.

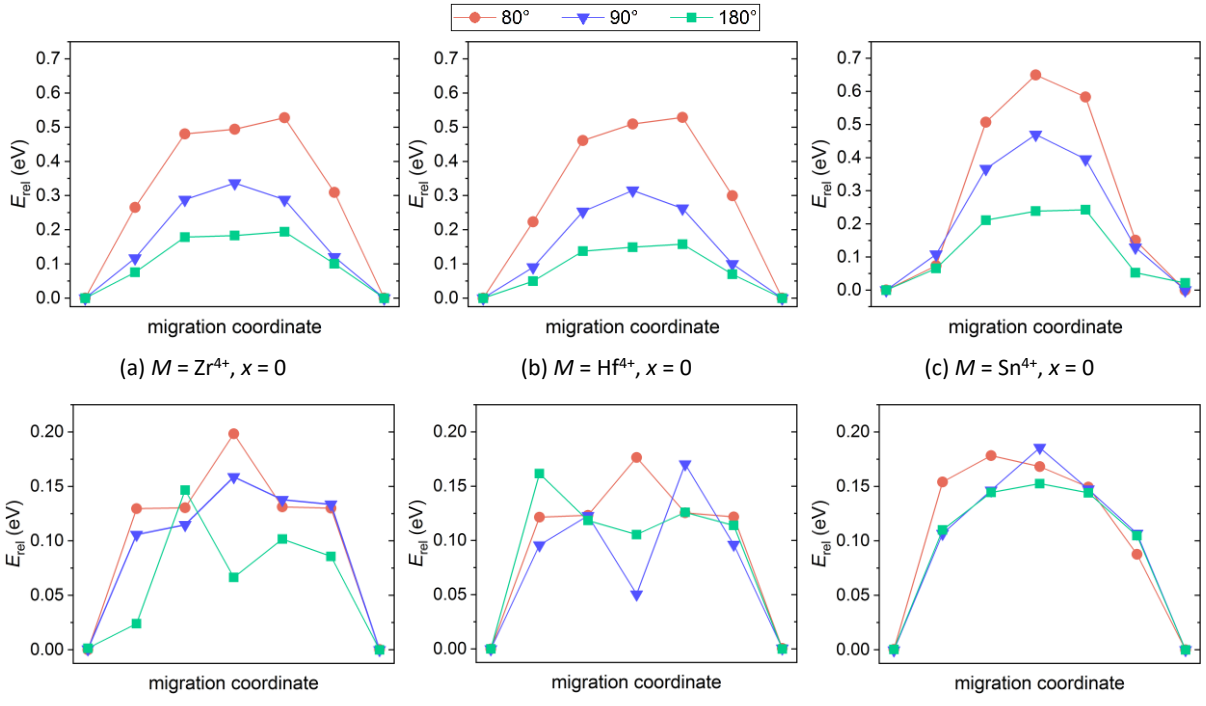

(a) M = Zr^{4+}, x = 0 (b) M = Hf^{4+}, x = 0 (c) M = Sn^{4+}, x = 0

(d) M = Zr^{4+}, x = 3 (e) M = Hf^{4+}, x = 3 (f) M = Sn^{4+}, x = 3

Figure S3. Energy profiles of migration pathways in 80° (red), 90° (blue) and 180° (green) in rhombohedral structure $Na_1M_2Si_xP_{3-x}O_{12}$ (M = Zr^{4+}, Hf^{4+}, Sn^{4+}) with x = 0 (a, b, c) and x = 3 (d, e, f).

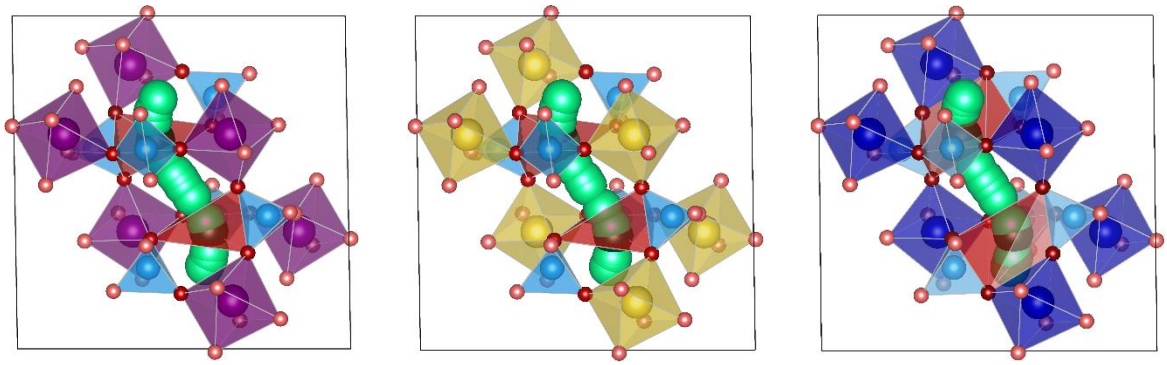

(a) M = Zr^{4+} (b) M = Hf^{4+} (c) M = Sn^{4+}

Figure S4. Coordination of the migrating Na^+ ions in the intermediate state in the structure $Na_4M_2Si_3O_{12}$ with (a) M = Zr^{4+}, (b) M = Hf^{4+}, (c) M = Sn^{4+}. The entire Na^+ migration path is shown in light green, the Na^+ positions in intermediate state in dark green. Key: Na (green), O (red), Zr/ZrO_6 (purple), Hf/HfO_6 (yellow), Sn/SnO_6 (dark blue), PO_4 (light blue).

The migration energies $E_{mig,0}$ of composition with M = Sn^{4+} are higher compared to those of M = Zr^{4+}, Hf^{4+}. However, the differences are largest at small substitution content x and decrease with increasing x. The differences in $E_{mig,0}$ can be explained, among others (see main text), by the different Na^+—O^{2-} bond distances shown in Table S4. The cell with M = Sn^{4+} exhibits a smaller volume (Fig. S2), resulting in smaller Na^+—O^{2-} bond distances for x = 0 compared to the cell with M = Zr^{4+}, Hf^{4+}. However, there are no significant differences in the bond distances for the compositions with x = 3. Here, the cell volume probably has little influence compared to the high number of Na^+ ions in the structures. At lower x, the fractional volume of the migrating Na^+ ions is smaller in M = Sn^{4+} than in M = Zr^{4+}, Hf^{4+}, leading to higher steric hindrance, which may explain the large differences in $E_{mig,0}$ among others.

Table S6. Averaged bond distances $\bar{d}_{Na1-O}$ between Na1 ions and O^{2-} in nearest neighbour positions and averaged bond distances $\bar{d}_{Na2-O}$ (Å) between Na2 ions and O^{2-} in nearest neighbour positions in $Na_1M_2Si_xP_{3-x}O_{12}$ (M = Zr^{4+}, Hf^{4+}, Sn^{4+}) with x = 0 and x = 3.

M	x = 0		x = 3	
	$\bar{d}_{Na1-O}$ (Å)	$\bar{d}_{Na2-O}$ (Å)	$\bar{d}_{Na1-O}$ (Å)	$\bar{d}_{Na2-O}$ (Å)
Zr^{4+}	2.53	2.77	2.35	2.79
Hf^{4+}	2.52	2.70	2.35	2.78
Sn^{4+}	2.46	2.63	2.36	2.76

5. Influences on migration energy

5.1 Na^+—Si^{4+} interaction

To determine the influence of the Na^+—Si^{4+} interactions on the migration energy, the amount of Si^{4+} ions near the migrating Na^+ ions in the structure $Na_1Zr_2P_3O_{12}$ (x = 0) is gradually increased. Fig. S5 shows the Si^{4+} sites (blue) to be occupied adjacent to the Na^+ migration path (green). With increasing number of Si^{4+} ions the migration energy decreases (see Fig. 7). The attractive interactions between the migrating Na^+ ion and the Si^{4+} ions decrease the migration energy due to stabilization of the transition state.

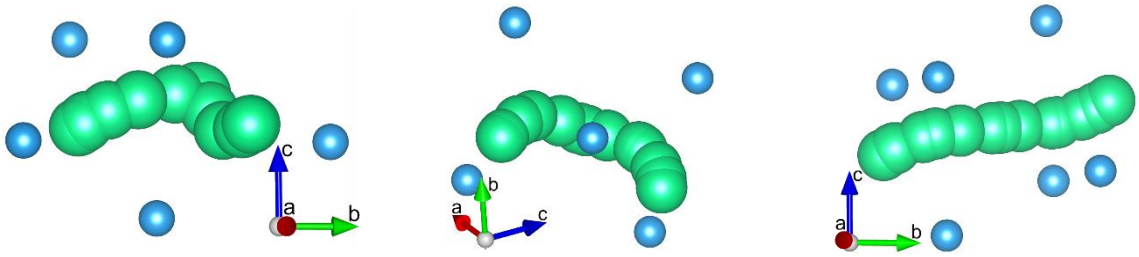

(a) 80° migration (b) 90° migration (c) 180° migration

Figure S5. Si^{4+} sites (blue) adjacent to the Na^+ migration pathway (green) in (a) 80°, (b) 90° and (c) 180°, which are gradually occupied to investigate the influence of the Na^+—Si^{4+} interactions on the migration energy.

5.2 Na^+—Na^+ interaction

To investigate the influence of the interactions between the migrating Na^+ ions and neighboring Na^+ ions on the migration energy, the amount of Na^+ ions near the migration pathway was gradually increased in the structure $Na_1Zr_2P_3O_{12}$ (x = 0). In Fig. S6, the migration pathway is shown in light green and the adjacent Na^+ sites in dark green. The calculated migration energies in dependence of the amount of Na^+ ions adjacent to the pathway are shown in Fig. S7. The results show no clear dependence of the migration energy on the number of Na^+ near the migration pathway. However, a dependence of the migration energy on the arrangement of Na^+ adjacent to the migration path is found. Occupying one Na site that is closest to the migration path and in the same plane results in the lowest migration energies. In the case of 80° migration, the occupation of site (3) and site (4) leads to the lowest migration energies of 0.29 eV and 0.32 eV, respectively. In the case of 90° migration, the occupation of site (1), site (2) and site (7) results in migration energies of 0.32 eV to 0.33 eV. But the occupation of the site (3) results in lower migration energy of 0.18 eV. This Na^+ site is below the migration path regarding the *a*/*c*-plane. In case of 180°, the migration energies are very similar. If more than one Na^+ site is occupied near the migration path, not only the arrangement of the occupied Na^+ sites with respect to the migration path, but also with respect to each other must be considered. However, a clear description cannot be given due to the complexity of the system.

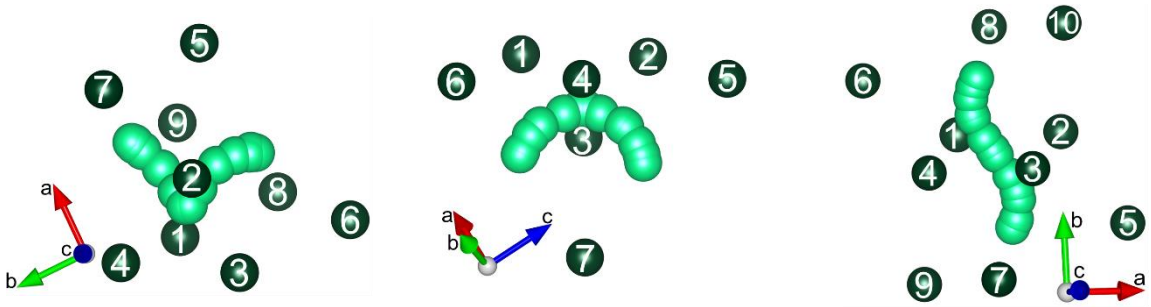

(a) 80° migration (b) 90° migration (c) 180° migration

Figure S6. Na^+ sites (dark green) adjacent to the Na^+ migration pathway (light green) in (a) 80°, (b) 90° and (c) 180°, which are gradually occupied to investigate the influence of the Na^+— Na^+ interactions on the migration energy.

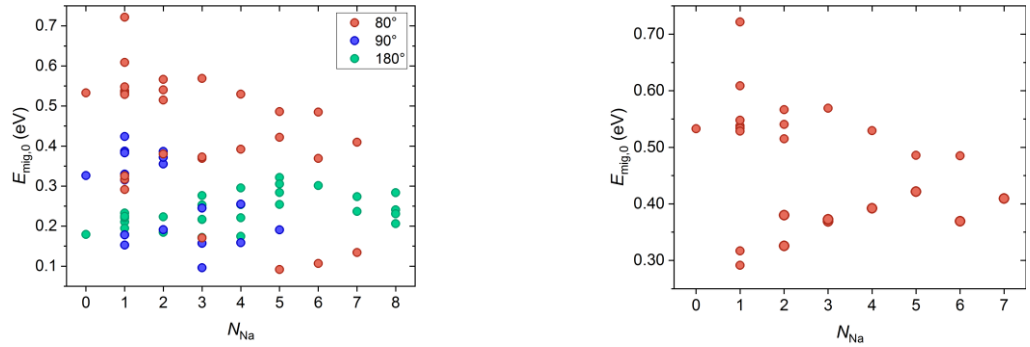

(a) Migration energies of 80°, 90°, 180° path

(b) Migration energies of 80° path

(c) Migration energies of 90° path

(d) Migration energies of 180° path

Figure S7. Migration energy $E_{mig,0}$ of the pathways in 80° (red), 90° (blue) and 180° (green) in dependence of the amount of Na^+ adjacent to the pathway in the structure with composition $Na_1Zr_2P_3O_{12}$. (a) $E_{mig,0}$ of all pathways, (b) $E_{mig,0}$ of the pathways in 80°, (c) $E_{mig,0}$ of the pathways in 90°, (d) $E_{mig,0}$ of the pathways in 180°.

5.3 Bottleneck

During the migration, the Na^+ ions pass through different bottlenecks formed by three O^{2+} ions of SiO_4/PO_4 tetrahedra and ZrO_6 octahedra. Fig. S8 shows the bottlenecks for the 180° migration path. The bottlenecks A and A' are located near the Na2 sites, while the bottlenecks B and B' are located near the Na1 site.

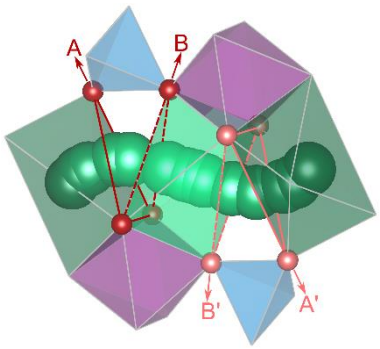

Figure S8. Bottlenecks formed by three O^{2+} ions of SiO_4/PO_4 tetrahedra and ZrO_6 octahedra for the case of the 180° migration pathway (grey). Key: Key: Na1 (light green), Na2 (dark green), O (red), SiO_4/PO_4 (blue), Zr/ZrO_6 (purple).

The four different bottlenecks of the migration paths are characterized by the size of their area. Fig. S9 shows the comparison of the bottleneck areas in non-substituted (x = 0) and fully substituted (x = 3) structure $Na_{1+x}M_2Si_xPi_{3-x}O_{12}$ with M = Zr^{4+}, Hf^{4+}, Sn^{4+}. A and A´ are larger for x = 3 compared to x = 0 whereas the bottleneck areas B and B' are similar for all compositions

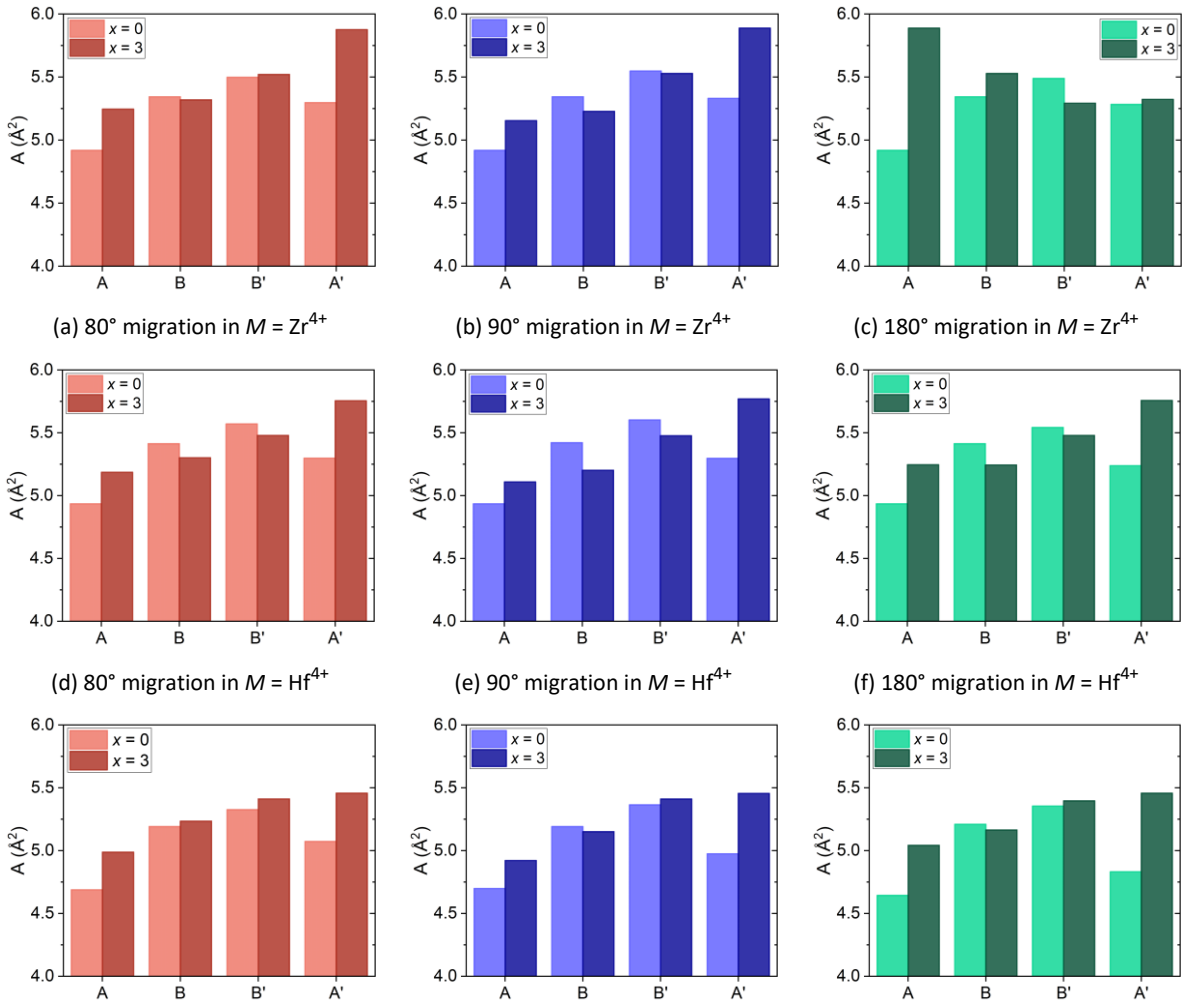

(a) 80° migration in M = Zr^{4+} (b) 90° migration in M = Zr^{4+} (c) 180° migration in M = Zr^{4+}

(d) 80° migration in M = Hf^{4+} (e) 90° migration in M = Hf^{4+} (f) 180° migration in M = Hf^{4+}

(g) 80° migration in M = Sn^{4+} (h) 90° migration in M = Sn^{4+} (i) 180° migration in M = Sn^{4+}

Figure S9. Size of bottleneck area of (a, d, g) 80°, (b, e, h) 90° and (c, f, i) 180° migration in the structure $Na_{1+x}M_2Si_xPi_{3-x}O_{12}$ (x = 0, 3) with (a, b, c) M = Zr^{4+}, (d, e, f) M = Hf^{4+}, (g, h, i) M = Sn^{4+}.

Fig. S10 shows the comparison of the bottleneck areas with respect to the compositions $Na_{1+x}M_2Si_xPi_{3-x}O_{12}$ (x = 0, 3) with the different M cations. In both structures with x = 0 and x = 3, the bottleneck areas are smaller in the composition with M = Sn^{4+} than M = Zr^{4+} and Hf^{4+}.

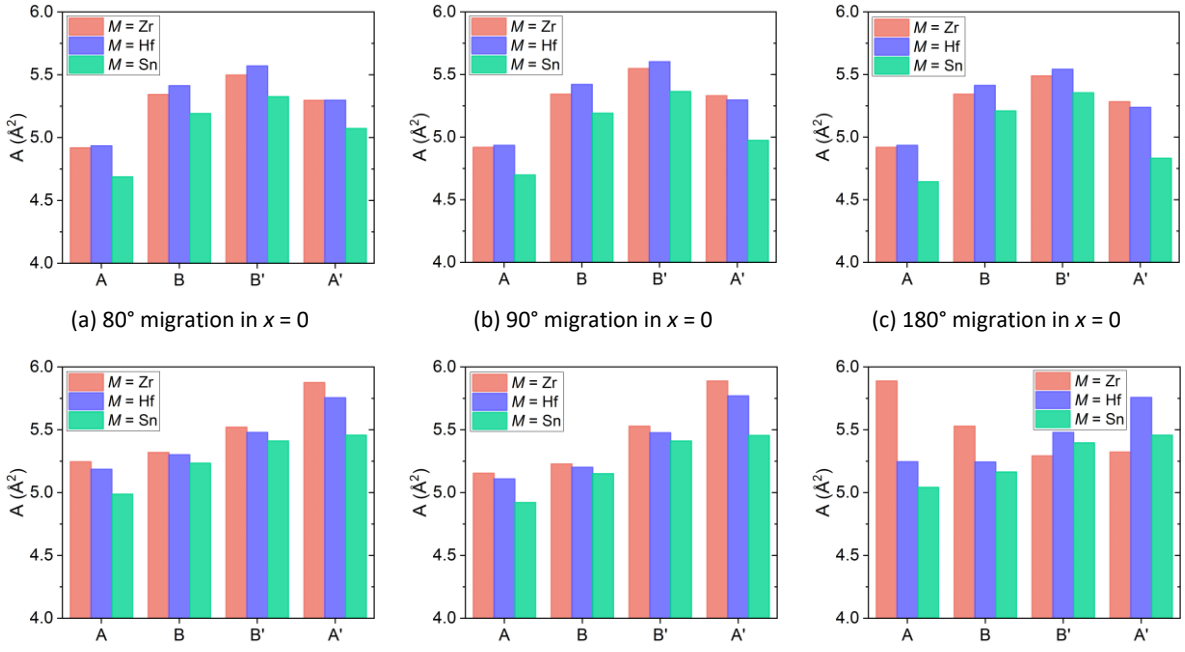

(a) 80° migration in x = 0 (b) 90° migration in x = 0 (c) 180° migration in x = 0

(d) 80° migration in x = 3 (e) 90° migration in x = 3 (f) 180° migration in x = 3

Figure S10. Size of bottleneck area of (a, d) 80°, (b, e) 90° and (c, f) 180° migration in the structure $Na_{1+x}M_2Si_xPi_{3-x}O_{12}$ with (a, b, c) x = 0 and (d, e, f) x = 3 and M = Zr^{4+} (red), M = Hf^{4+} (blue), M = Sn^{4+} (green).

6. Ionic conductivity

Fig. S11 shows the conductivity depending on substitution level x of $Na_{1+x}M_2Si_xP_{3-x}O_{12}$ with M = Zr^{4+}, Hf^{4+}, Sn^{4+} obtained from KMC simulations where the Na^+–cation pair interactions are not considered. The conductivities of all compositions are very similar. The slightly lower conductivities of the composition with M = Sn^{4+} compared to those of the composition with M = Zr^{4+}, Hf^{4+}, and the small shift in conductivity maximum can be explained by the differences in migration energies $E_{mig,0}$.

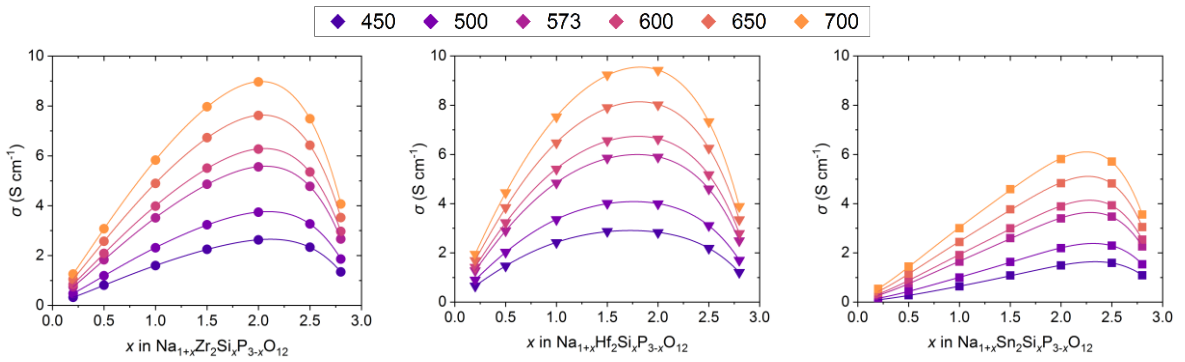

(a) M = Zr^{4+} (b) M = Hf^{4+} (c) M = Sn^{4+}

Figure S11. Na^+ conductivity dependent on substitution content x of $Na_{1+x}M_2Si_xP_{3-x}O_{12}$ ($0.2 \le x \le 2.8$) with (a) M = Zr^{4+}, (b) M = Hf^{4+}, (c) M = Sn^{4+} in temperature range of $450 \le T \le 700$ in 10 × 10 × 10 cell obtained from simulations where sodium–cation pair interactions are not considered.

The simulated ionic conductivities of $Na_{1+x}M_2Si_xPi_{3-x}O_{12}$ ($0.01 \le x \le 2.8$) with $M = Zr^{4+}$, Hf^{4+}, Sn^{4+} show the temperature dependence according to the Arrhenius equation as shown in in Fig. S12.

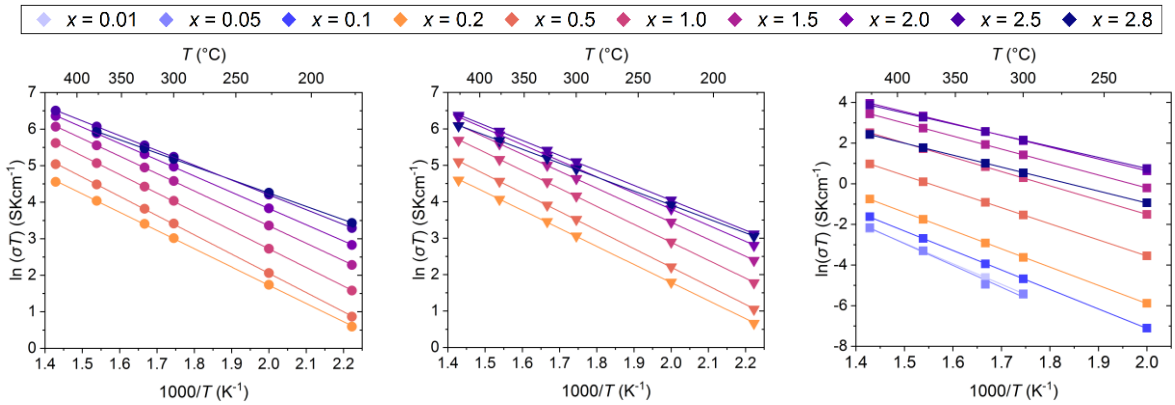

(a) $M = Zr^{4+}$ (b) $M = Hf^{4+}$ (c) $M = Sn^{4+}$

Figure S12. Arrhenius plot obtained from simulated conductivities of $Na_{1+x}M_2Si_xPi_{3-x}O_{12}$ with (a) $M = Zr^{4+}$ ($0.2 \le x \le 2.8$), (b) $M = Hf^{4+}$ ($0.2 \le x \le 2.8$), (c) $M = Sn^{4+}$ ($0.01 \le x \le 2.8$)in the temperature range of $450 \le T \le 700$ in $10 \times 10 \times 10$ cell.

References

1 J. Schuett, F. Pescher and S. Neitzel-Grieshammer, The origin of high Na^+ ion conductivity in $Na_{1+x}Zr_2Si_xP_{3-x}O_{12}$ NASICON materials, *Phys. Chem. Chem. Phys.*, 2022, **24**, 22154–22167.

2 C. Delmas, R. Olazcuaga, G. Le Flem, P. Hagenmuller, F. Cherkaoui and R. Brochu, Crystal chemistry of the $Na_{1+x}Zr_{2-x}L_x(PO_4)_3$ (L=Cr, In, Yb) solid solutions, *Mater. Res. Bull.*, 1981, **16**, 285–290.

3 J. Alamo, Chemistry and properties of solids with the [NZP] skeleton, *Solid State Ion.*, 1993, **63**, 547–561.

4 E. M. Vogel, R. J. Cava and E. Rietman, Na^+ ion conductivity and crystallographic cell characterization in the Hf-NASICON system $Na_{1+x}Hf_2Si_xP_{3-x}O_{12}$, *Solid State Ion.*, 1984, **14**, 1–6.

5 H. Aono and E. Suginoto, Ionic conductivity and sinterability of NASICON-type ceramics: The systems $NaM_2(PO_4)_3$+yNa_2O (M=Ge, Ti, Hf, and Zr), *J. Am. Ceram. Soc.*, 1996, **79**, 2786–2788.

6 M. P. Carrasco, M. C. Guillem and J. Alamo, Structural study, thermal expansion and electrical conductivity of the composition $NaSnZr(PO_4)_3$, *Solid State Ion.*, 1993, **63**, 688–691.

7 J. L. Rodrigo and J. Alamo, Phase transition in $NaSn_2(PO_4)_3$ and thermal expansion of $NaM_2^{IV}(PO_4)_3$; M^{IV}=Ti, Sn, Zr, *Mater. Res. Bull.*, 1991, **26**, 475–480.

8 E. R. Losilla, M. A. G. Aranda, S. Bruque, M. A. París, J. Sanz and A. R. West, Understanding Na mobility in NASICON materials: A Rietveld, 23Na and 31P MAS NMR, and impedance study, *Chem. Mater.*, 1998, **10**, 665–673.

9 Z. Zou, N. Ma, A. Wang, Y. Ran, T. Song, Y. Jiao, J. Liu, H. Zhou, W. Shi and B. He, Relationships between Na^+ distribution, concerted migration, and diffusion properties in rhombohedral NASICON, *Adv. Energy Mater.*, 2020, **10**, 2001486.

10 Z. Zhang, Z. Zou, K. Kaup, R. Xiao, S. Shi, M. Avdeev, Y.-S. Hu, Da Wang, B. He and H. Li, Correlated migration invokes higher Na^+-ion conductivity in NASICON-type solid electrolytes, *Adv. Energy Mater.*, 2019, **9**, 1902373.

11 Z. Zou, N. Ma, A. Wang, Y. Ran, T. Song, B. He, A. Ye, P. Mi, L. Zhang and H. Zhou, Identifying migration channels and bottlenecks in monoclinic NASICON-type solid electrolytes with hierarchical ion-transport algorithms, *Adv. Funct. Mater.*, 2021, **31**, 2107747.

12 J.-P. Boilot, G. Collin and P. Colomban, Relation structure-fast ion conduction in the NASICON solid solution, *J. Solid State Chem.*, 1988, **73**, 160–171.

13 J. J. Shi, G. Q. Yin, L. M. Jing, J. Guan, M. P. Wu, Y. L. Zhou, H. L. Lou and Z. Wang, Lithium and sodium diffusion in solid electrolyte materials of $AM_2(PO_4)_3$ (A=Li, Na, M=Ti, Sn and Zr), *Int. J. Mod. Phys. B*, 2014, **28**, 1450176.

14 F. Cherkaoui, G. Villeneuve, C. Delmas and P. Hagenmuller, Sodium motion in the NASICON related $Na_{1+x}Zr_{2-x}In_x(PO_4)_3$ solid solution: An NMR study, *J. Solid State Chem.*, 1986, **65**, 293–300.